Supporting Information

Investigation of the Reversible Intercalation/Deintercalation of Al into the Novel Li_3VO_4@C Microsphere Composite Cathode Material for Aluminum-Ion Batteries

*Jiali Jiang, He Li, Jianxing Huang, Kun Li, Jing Zeng, Yang Yang, Jiaqi Li, Yunhui Wang, Jing Wang and Jinbao Zhao**

State Key Laboratory of Physical Chemistry of Solid Surfaces, Collaborative Innovation Center of Chemistry for Energy Materials, State-Province Joint Engineering Laboratory of Power Source Technology for New Energy Vehicle, College of Chemistry and Chemical Engineering, Xiamen University, No. 422 Siming South Road, Xiamen, Fujian 361005, China

*Corresponding author

Tel: 0086-592-2186935

E-mail: jbzhao@xmu.edu.cn

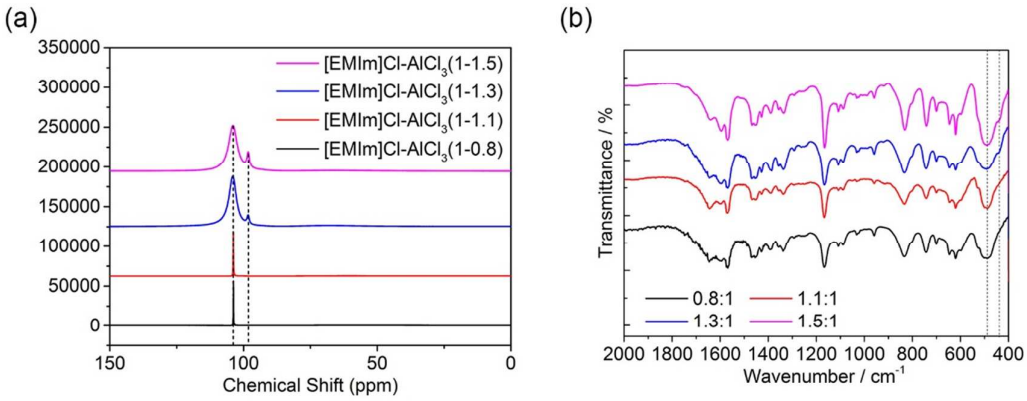

Figure S1. The physical characteristics of the as-prepared ($[EMIm]Al_xCl_y$) ionic liquids with different $AlCl_3$/[EMIm]Cl ratio. (a) ^{27}Al NMR spectra, (b) FTIR spectra of ionic liquid [EMIm]Cl-$AlCl_3$ with different mole ratio of $AlCl_3$/[EMIm]Cl varies from 0.8 to 1.5.

It is clearly seen from the Figure S1a, one strong peak at 103.95 ppm can be assigned to $AlCl_4^-$.[1] When the $AlCl_3$/[EMIm]Cl mole ratio is higher than 1.1 : 1, the peak at 98.15 ppm, which represents anion $Al_2Cl_7^-$, emerges,[1] and becomes stronger with increasing mole ratio. The ratio of $AlCl_4^-$ to $Al_2Cl_7^-$ is 6.98 : 1 in the $AlCl_3$/[EMIm]Cl = 1.3 ionic liquid, but the ratio decreases to 4.66 : 1 in the $AlCl_3$/[EMIm]Cl = 1.5 ionic liquid, which means the addition of $Al_2Cl_7^-$. The same result also can be got from the Figure S1b. It shows the FTIR spectra of ionic liquid with different mole ratio, which are very similar above 500 cm^{-1}, because they have the same cations. But the vibration intensity of Al-Cl bonds at 490 cm^{-1} increases with the increment of $AlCl_3$: [EMIm]Cl mole ratio. The peak at 440 cm^{-1} appears when the mole ratio is higher than 1.1 : 1, and becomes stronger as the mole ratio increasing, which can be ascribed to the vibration of Al-Cl-Al bonds in $Al_2Cl_7^-$ or larger chloroaluminate species.[2] Based on the results discussed above, we can conclude that increased $AlCl_3$ contents lead to the emergence of larger chloroaluminate complex anions ($Al^- \rightarrow AlCl_4^- \rightarrow Al_2Cl_7^- \rightarrow Al_3Cl_{10}^-$…), and both $AlCl_4^-$ and $Al_2Cl_7^-$ anions exist in the $AlCl_3$/[EMIm]Cl ratio of 1.3, with the ratio $[AlCl_4^-]/[Al_2Cl_7^-] \approx 6.98 : 1$.

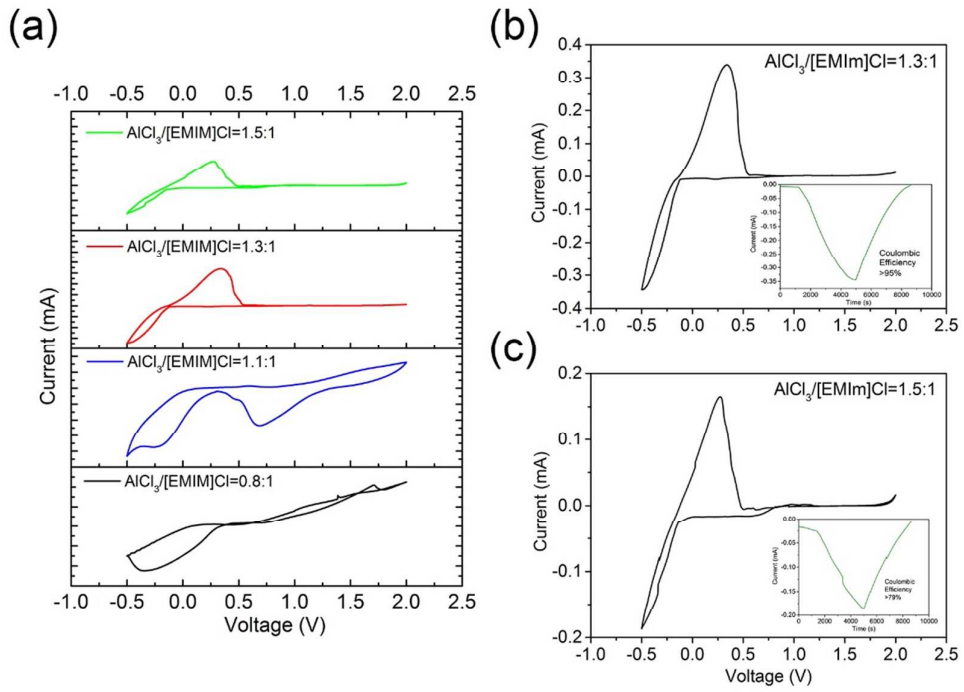

Figure S2. The electrochemical properties of room-temperature ionic liquids with different $AlCl_3$/[EMIm]Cl ratio. (a) Cyclic voltammograms of ionic liquid [EMIm]Cl-$AlCl_3$ with different ratio. Al deposition/stripping in (b) $AlCl_3$/[EMIm]Cl = 1.3 electrolyte and (c) $AlCl_3$/[EMIm]Cl = 1.5 electrolyte, insets: charge-time curves of Al deposition/stripping. Scan rate: 0.1 mV s^{-1}, working electrode (WE): Au foil; counter electrode (CE) and reference electrode (RE): Al foil.

It can be analyzed from Figure S2a that the neutral ionic liquid ($AlCl_3$/[EMIm]Cl = 1.1) and the basic ionic liquid ($AlCl_3$/[EMIm]Cl = 0.8) show no electrochemical reversibility in Al-ion battery. And there is a pair of distinct redox peaks in the cyclic voltammograms of acidic ionic liquids (the $AlCl_3$/[EMIm]Cl ratio is higher than 1.1). When the voltage is lower than -0.1 V (vs. Al reference electrode), the cathodic peak corresponds to the reduction process of $Al_2Cl_7^-$ to Al, and the generated aluminum will deposit on the surface of the Al anode. The anodic peak at 0.25 V (vs. Al reference electrode) can be attributed to the stripping of Al anode in the acidic ionic liquid electrolyte.[3] Figure S2b and Figure S2c show the Al deposition/stripping curve in [EMIm]Cl: $AlCl_3$ = 1 : 1.3 electrolyte and [EMIm]Cl: $AlCl_3$=1 : 1.5 electrolyte, and the charge balance curve (inset of Figure S2b) manifests the deposition/stripping process is highly reversible with a coulombic efficiency greater than 95% in the electrolyte with the $AlCl_3$/[EMIm]Cl ratio of 1.3. Nevertheless, as the contents of $AlCl_3$ increases, the intensities of peak current decrease sharply and the coulombic efficiency of deposition/stripping process declines steeply to approximately 79%. As a whole, the electrolyte with the $AlCl_3$/[EMIm]Cl ratio of 1.3 indicates the excellent

performance of electrodeposition of aluminum, which makes the ($[EMIm]Al_xCl_y$) ionic liquid with the $AlCl_3$/[EMIm]Cl ratio of 1.3 be the optimal proportion for Al-ion battery electrolytes.

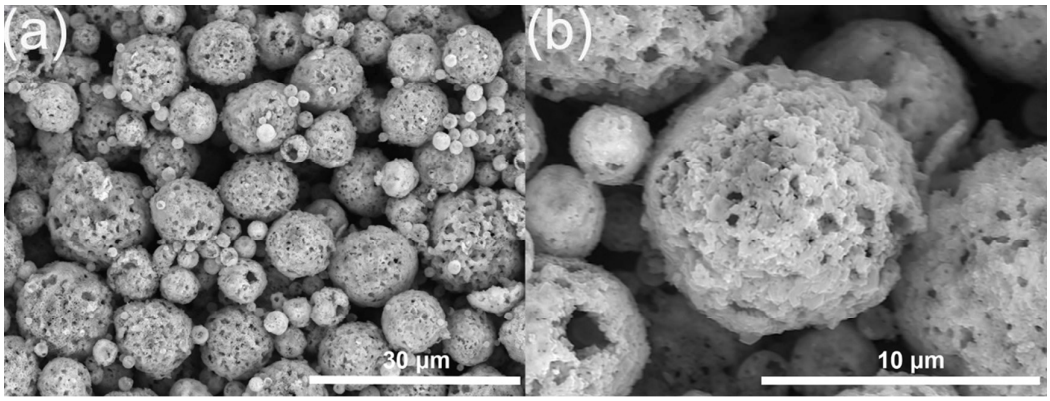

Figure S3. (a) Low magnification SEM image and (b) high magnification SEM image of Li_3VO_4.

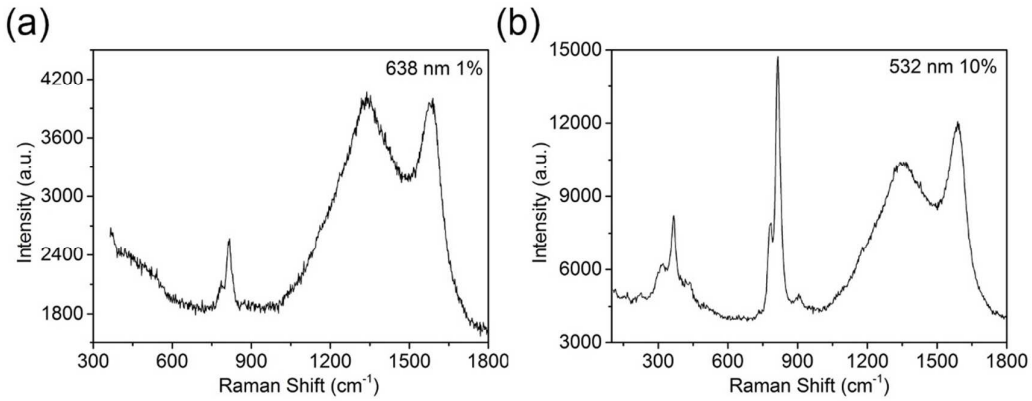

Figure S4. Raman spectra of Li_3VO_4@C powders with (a) laser wave length: 638 nm, laser intensity: 1% of the maximum 200 mW, collection time constant: 20 s. (b) laser wave length: 532 nm, laser intensity: 10% of the maximum 200 mW, collection time constant: 20 s.

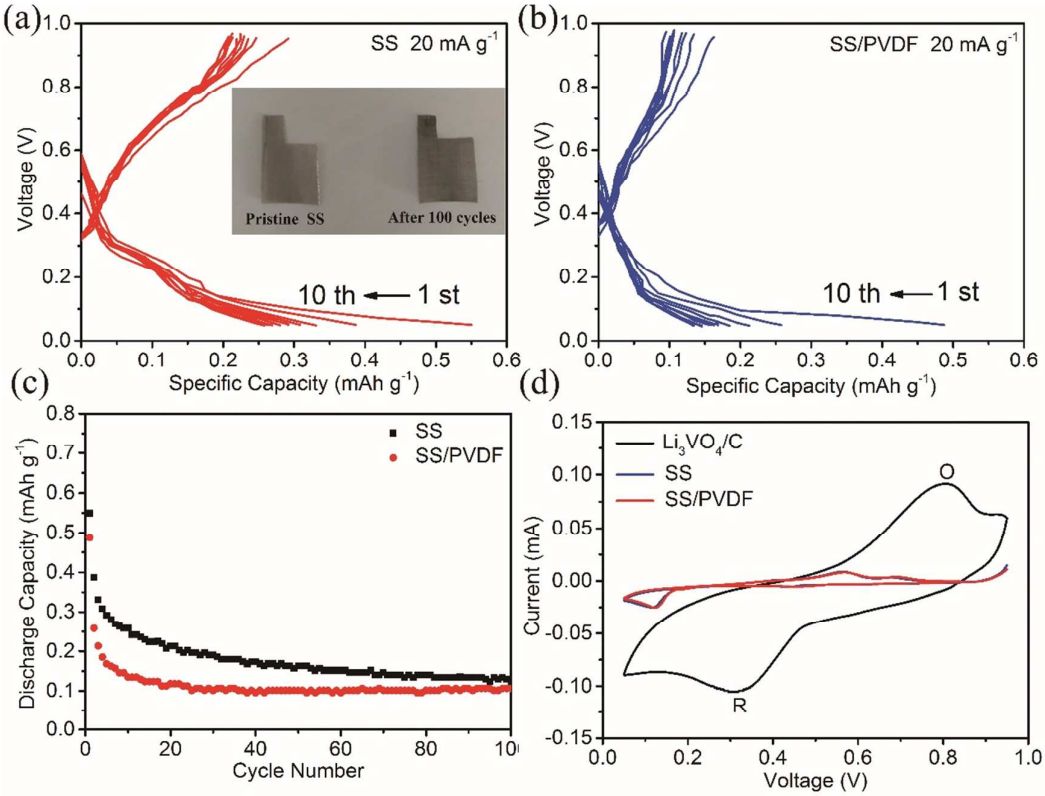

Figure S5. Electrochemical characterization of stainless-steel mesh and PVDF in acidic ionic liquid. Galvanostatic discharge-charge profiles of (a) stainless-steel mesh and (b) PVDF at a current density of 20 mA g^{-1} from the first to the tenth cycle, inset of (a): photographs of stainless-steel mesh before discharge (left) and after 100 cycles (right). (c) Cycle performance of stainless steel and PVDF at a current density of 20 mA g^{-1}. All capacity calculations are based on the average mass of Li_3VO_4@C, and the mass is set for 2.35 mg, between 2.0 mg and 2.5 mg. (d) Cyclic voltammograms of Li_3VO_4@C, stainless steel and PVDF at 0.1 mV s^{-1}.

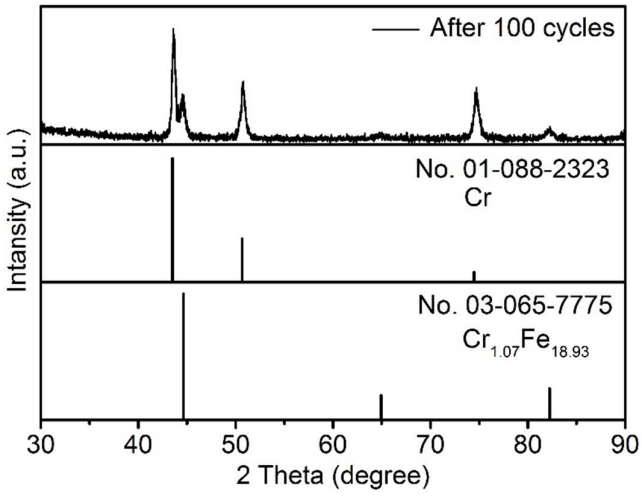

Figure S6. XRD pattern of stainless-steel mesh after 100 cycles in acidic ionic liquid.

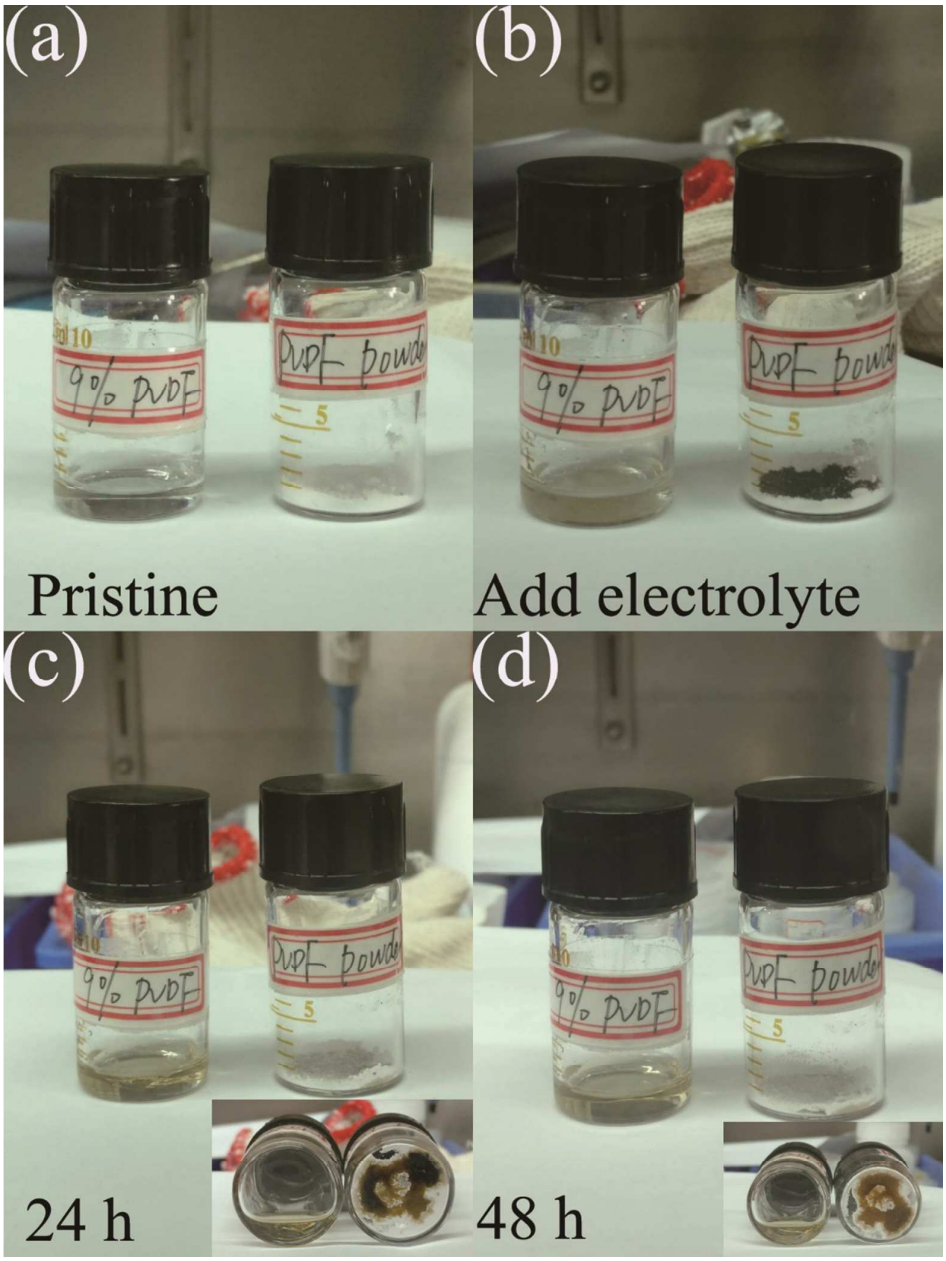

Figure S7. The changes in color before and after adding acidic electrolyte into PVDF (9 wt% in NMP) and PVDF powders. (a) pristine PVDF (9 wt% in NMP) and PVDF powders. (b) The changes in color instantly after adding 100 μL acidic electrolyte. Standing for (c) 24 h and (d) 48 h.

Reed and Menke have convincingly argued that V_2O_5 is electrochemically inert in $AlCl_3$-EMIC electrolyte.[4] The galvanostatic cycling profiles and cyclic voltammograms of stainless steel both indicate the identical electrochemical performance with Al-V_2O_5 cells.[5] Therefore, the electrochemical activities of Al-V_2O_5 cells are ascribes to the reversible corrosion reactions of Fe and Cr with the acidic

$AlCl_3$-EMIC, rather than Al^{3+} ion intercalation/deintercalation processes in V_2O_5. To exclude the influence of stainless-steel mesh in electrochemical performance of Li_3VO_4@C batteries. Soft package batteries were assembled with stainless steel as current collector, and with no active material. As shown in figure S5a, the specific capacity of stainless steel in acidic $AlCl_3$-[EMIM]Cl ($AlCl_3$: [EMIM]Cl = 1.3 : 1) is almost negligible and there is no electrochemical platform in galvanostatic discharge-charge profiles (All capacity calculations are based on the average mass of Li_3VO_4@C, and the mass is set for 2.35 mg, between 2.0 mg and 2.5 mg.). The comparison of CV curves (Figure S5d) between stainless steel and Li_3VO_4@C also verify that the tiny effect of stainless steel on the electrochemical performance of Li_3VO_4@C-Al batteries. To further analyze the changes of stainless steel before and after 100 cycles, XRD test was carried out, as indicated in figure S6. The diffraction lines of stainless steel after 100 cycles perfectly match with the Cr (JCPDS No. 01-088-2323) and $Cr_{1.07}Fe_{18.93}$ (JCPDS No. 03-065-7775). No apparent diffraction lines of iron chloride and chromium chloride can be observed, which means there is no electrochemical reaction between stainless steel and acidic ionic liquid electrolyte.

In addition, Wang and co-workers added white PVDF and PTFE powders to prepared acidic chloroaluminate ionic liquid ($AlCl_3$/[BMIM]Cl = 1.1:1) to investigate the effect of acidic ionic liquid on PVDF (Polyvinylidene Fluoride), and found the $Al_2Cl_7^-$ in ionic liquid reacts with PVDF.[6] To further enrich the in-depth understanding of relationship between PVDF and acidic ionic liquid, a series of experiments were also operated. PVDF binder (9 wt% in NMP) was directly coated on 1 cm×1 cm stainless-steel mesh, the amount of PVDF is equal to the amount of PVDF in Li_3VO_4 electrode, then the stainless-steel electrodes were dried in vacuum oven at 60 ^oC overnight to remove residual NMP. The soft package batteries were then assembled. the electrochemical performance is shown in figure S5b, which manifests the electrochemical curves of PVDF in acidic $AlCl_3$-[EMIM]Cl ($AlCl_3$: [EMIM]Cl = 1.3 : 1) is similar to stainless steel (Figure S5a), likewise, the specific capacity is negligible and there is no electrochemical platform in galvanostatic discharge-charge profiles. CV curve of PVDF (Figure S5d) is also analogous to stainless steel. It can be concluded that PVDF has basically no effect on electrochemical performance of Li_3VO_4@C-Al cells. Besides, the changes in color before and after adding acidic ionic liquid into PVDF (9 wt% in NMP) and PVDF powders were also explored. The net content of PVDF are both 0.1 g, and the amount of acidic ionic liquid are both 100 μL. It is clearly shown from figure S7 that the PVDF powders darkened rapidly when ionic liquid was added, and maintained black after standing for 24 h, even 48 h. However, adding the same amount of acidic ionic liquid into PVDF (9 wt% in NMP), then slightly shake the bottle, the colorless liquid turned pale yellow, which is similar

to color of acidic $AlCl_3$-[EMIM]Cl electrolyte. The color did not change after standing for long time. The obtained results above can be attributed to the physical and chemical properties of PVDF (9 wt% in NMP) are more stable than PVDF powders, the main reason may be the degree of polymerization and crosslinking of PVDF increased when PVDF powders mixed with NMP by magnetic stirring, therefore, it can maintain stability in acidic ionic liquid for long time. The Li_3VO_4@C electrode after 100 cycles (Figure S15c) indicates the active material did not fall off from current collector, which also illustrates that the PVDF binder can maintain stability in acidic ionic liquid for long cycling.

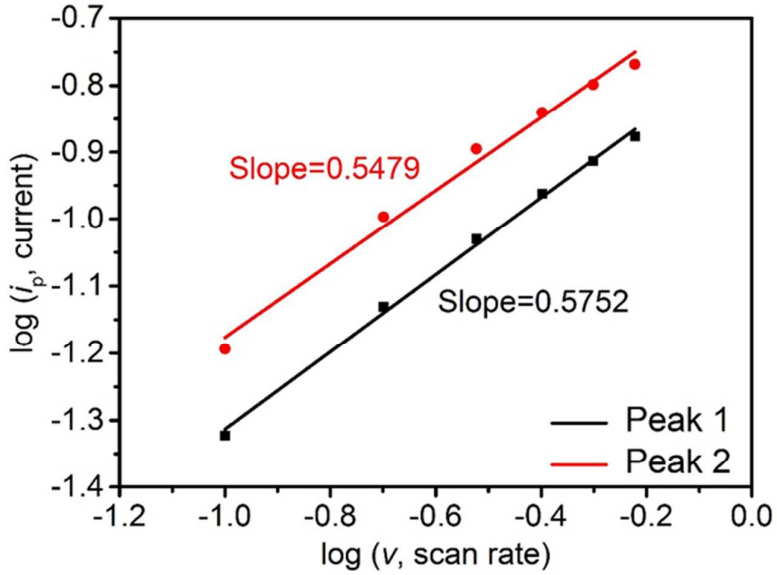

Figure S8. Log(i_p) versus log(v) plots at different redox states of the Li_3VO_4@C.

According to Randles-Sevcik equation, the relationship between peak current (i_p) and scan rate (v) can be described by the equations as follows:

$$i_p = a v^b \quad (1)$$

$$\log(i_p) = b\log(v) + \log(a) \quad (2)$$

where i_p is the peak current, v is the scan rate, and a and b are the adjustable parameters. The b value determines the type of Al^{3+} insertion/extraction. When b = 0.5, the electrochemical reaction is controlled by ionic diffusion, and when b = 1, the process mainly depends on pseudocapacitive control.[7] Figure S8 demonstrates the

linear relationship between log(i_p) and log(v) plots at different redox states. The b values of peak 1 (reduction) and peak 2 (oxidation) are 0.5752 and 0.5479, respectively, approximate to 0.5, which illustrates the discharge/charge process of Li_3VO_4@C are mainly ionic diffusion controlled. Therefore, Randles-Sevcik equation can be used to approximately calculate the ionic diffusion coefficient in Li_3VO_4@C-Al battery system. The detailed calculation process of aluminum ion diffusion coefficient in initial discharge is as follows:

The Al^{3+} concentration is obtained by amount of intercalation in the initial cycle, and the amount of intercalation is calculated by specific discharge capacity of initial cycle. The average mass of active material is 2.35 mg, according to our previous work,[8] the carbon ratio of the Li_3VO_4@C composite was estimated to be 24.0% by thermogravimetric analysis, hence the mass of Li_3VO_4 is 2.35×76.0% = 1.786 mg, and the molar of Li_3VO_4 is $1.786/135.6\times10^{-3} = 1.317\times10^{-5}$ mol.

The initial discharge capacity of Li_3VO_4@C electrode is 137 mAh g^{-1}, and the theoretical specific capacity is 591 mAh g^{-1} (calculated by intercalation of per molecule aluminum into the active material), therefore, the value of x in $Al_xLi_3VO_4$ is 137/591 = 0.2318. and the amount of aluminum in the electrode is $1.317\times10^{-5}\times0.2318 = 3.053\times10^{-6}$ mol.

The thickness and the area of active material is 10 μm and 1 cm^2, respectively. Therefore, the parameter C, which stands for Al^{3+} concentration in the electrode, is $3.053\times10^{-6}/1\times0.001 = 3.053\times10^{-3}$ mol/cm^3.

And according to Randles-Sevcik equation:

$$i_p = 0.4463nFAC\left(\frac{nF\nu D}{RT}\right)^{\frac{1}{2}}$$

The apparent diffusion coefficient of reduction peak 1 of Li_3VO_4@C electrode is calculated to be 1.928×10^{-12} cm^2 s^{-1}, likewise, the apparent diffusion coefficient of reduction peak 1 of Li_3VO_4 electrode is calculated to be 2.233×10^{-13} cm^2 s^{-1}.

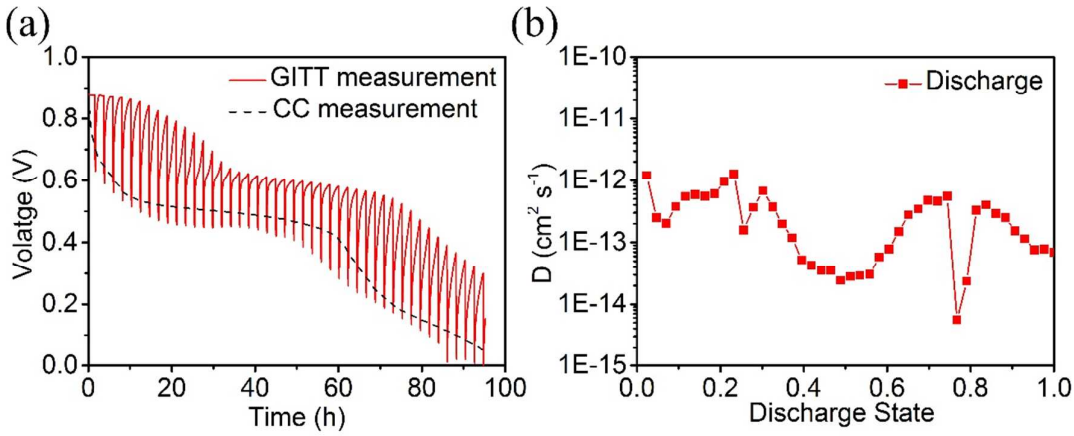

Figure S9. (a) The comparison of GITT measurement and corresponding constant current (CC) measurement of Li_3VO_4@C electrode. (b) The calculated aluminum ion diffusion coefficients from GITT curve.

In a typical GITT measurement, the battery was discharged with a current impulse with the current density of 20 mA g^{-1} for an interval τ of 600 seconds followed by an open circuit standing for 2 hours. Figure S9a exhibits the comparison of GITT and constant current (CC) measurement of the initial discharge process of Li_3VO_4@C electrode. The GITT curve matches well with the CC curve, where one plateau around 0.5 V can be observed. According to equation (3), the Al-ion diffusion coefficients in Li_3VO_4@C electrode at different discharge states can be determined using GITT data.[9]

$$D_{Al^{3+}} = \frac{4}{\pi}\left(\frac{iV_m}{zFA}\right)^2\left(\frac{dE_S/dt_S}{dE_\tau/d\tau^{1/2}}\right)^2 \approx \frac{4}{9\pi\tau}\left(\frac{mV_m}{MA}\right)^2\left(\frac{\Delta E_S}{\Delta E_\tau}\right)^2 \quad \left(\tau \ll \frac{L^2}{D_{Al^{3+}}}\right) \qquad (3)$$

where *i* is the current (A), V_m is the molar volume (cm^3 mol^{-1}) of Li_3VO_4, z is the charge number (z = 3 for Al^{3+} ion), F is the Faraday's constant, A is the effective surface area (cm^2) between the active material and the electrolyte, E_s is the steady state potential (V) measured during the rest time t_s (s) and E_τ is the potential (V) measured during the current pulse of duration τ (s). m and M are the mass (g) and the molecular weight (g mol^{-1}) of the active material, respectively. and L is the thickness of the electrode (cm). ΔE_s is the change of steady-state potential after a discharge pulse and open circuit standing, while ΔE_τ is the voltage change during a discharge pulse. The calculated D values are shown in Figure S9b. the aluminum ion diffusion coefficients of Li_3VO_4@C electrode lie in 1.198×10^{-12} - 5.557×10^{-15} cm^2 s^{-1}. This result is comparable with the apparent diffusion coefficients obtained from CV tests.

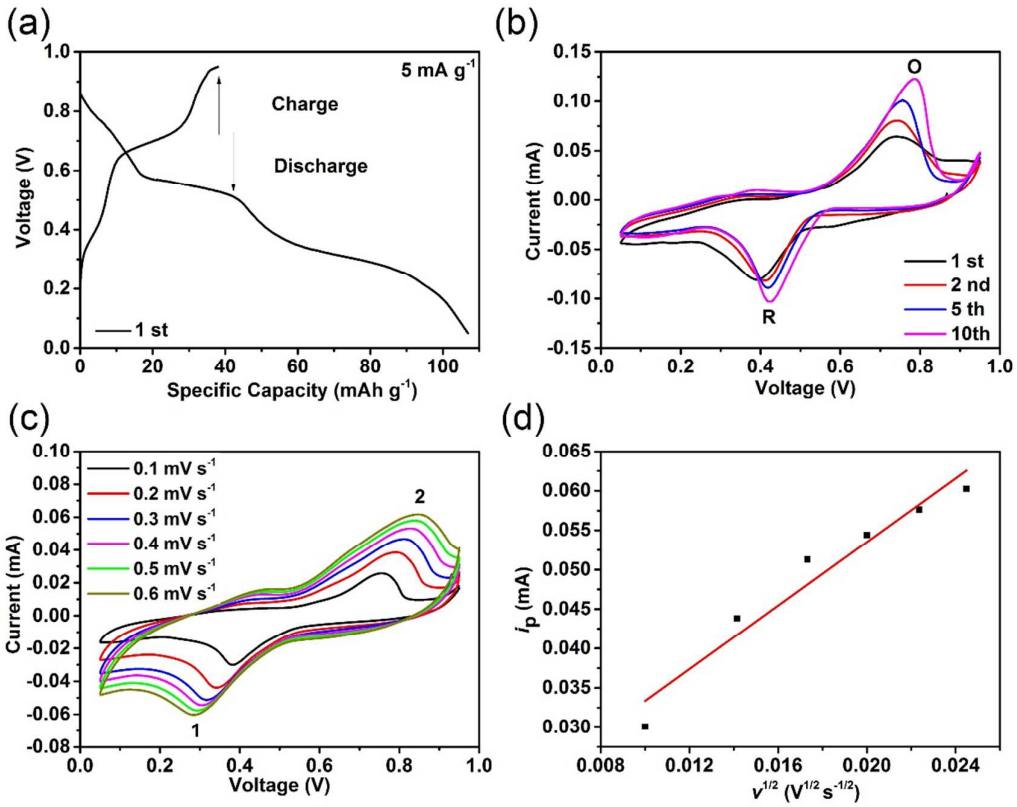

Figure S10. Electrochemical performance and kinetic study of pristine Li_3VO_4/Al batteries. (a) Initial discharge/charge curve at a current density of 20 mA g^{-1}. (b) Cyclic voltammogram at a scan rate of 0.1 mV s^{-1}. (c) Cyclic voltammograms at different scan rates. (d) Fitted line of i_p and $v^{1/2}$.

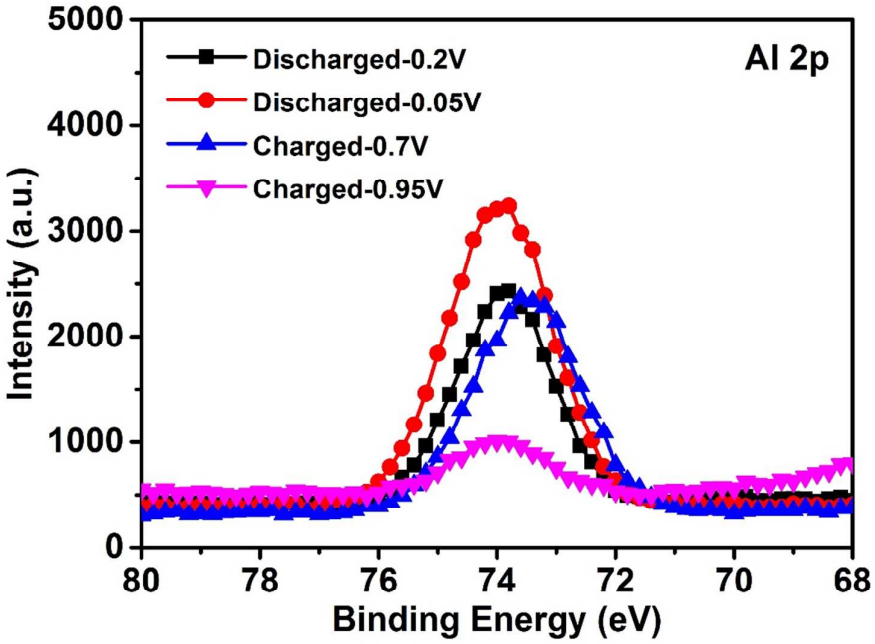

Figure S11. Aluminum content analysis of the Li_3VO_4@C electrode in the first cycle. XPS spectra of Al 2p in different discharge states.

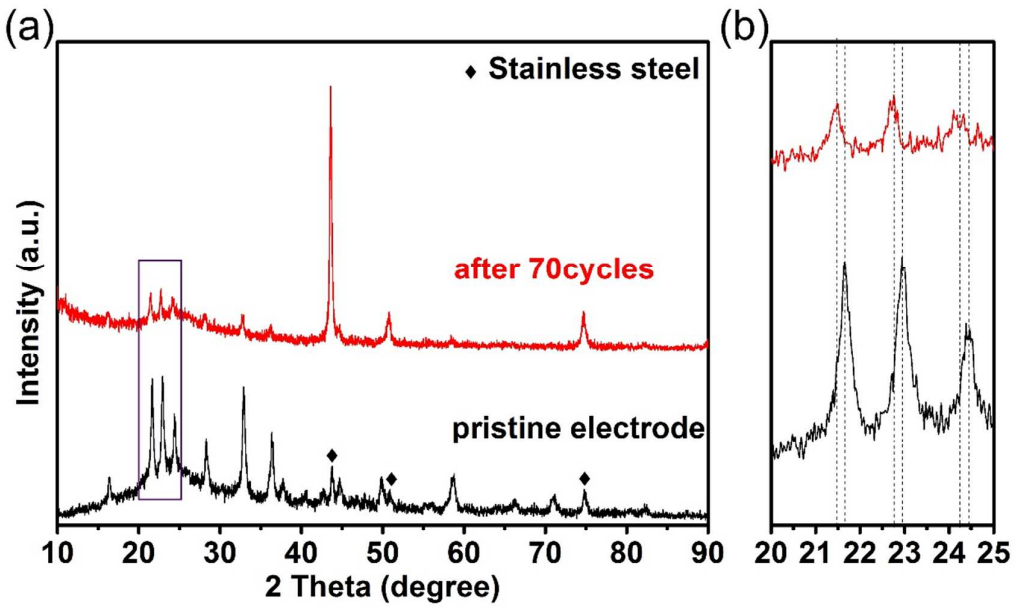

Figure S12. (a) XRD patterns of original Li_3VO_4@C electrode and Li_3VO_4@C electrode after 70 cycles. (b) The enlargement of selected region.

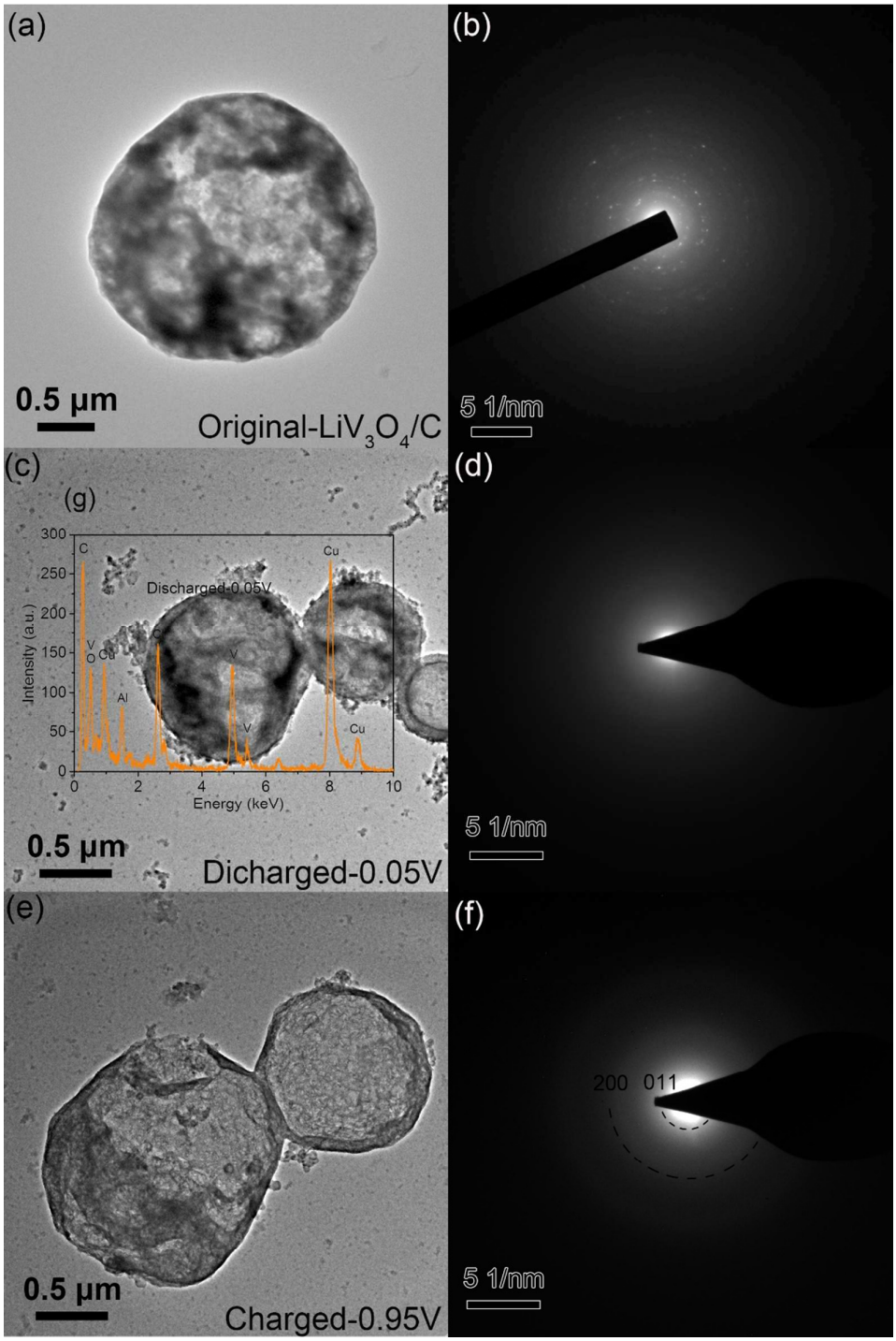

Figure S13. (a), (c) and (e) TEM images of original Li_3VO_4@C, discharged to 0.05 V, charged to 0.95 V in the initial cycle, respectively. (b), (d) and (f) SAED patterns corresponding to (a), (c) and (e). (g) EDS spectrum of discharged to 0.05 V.

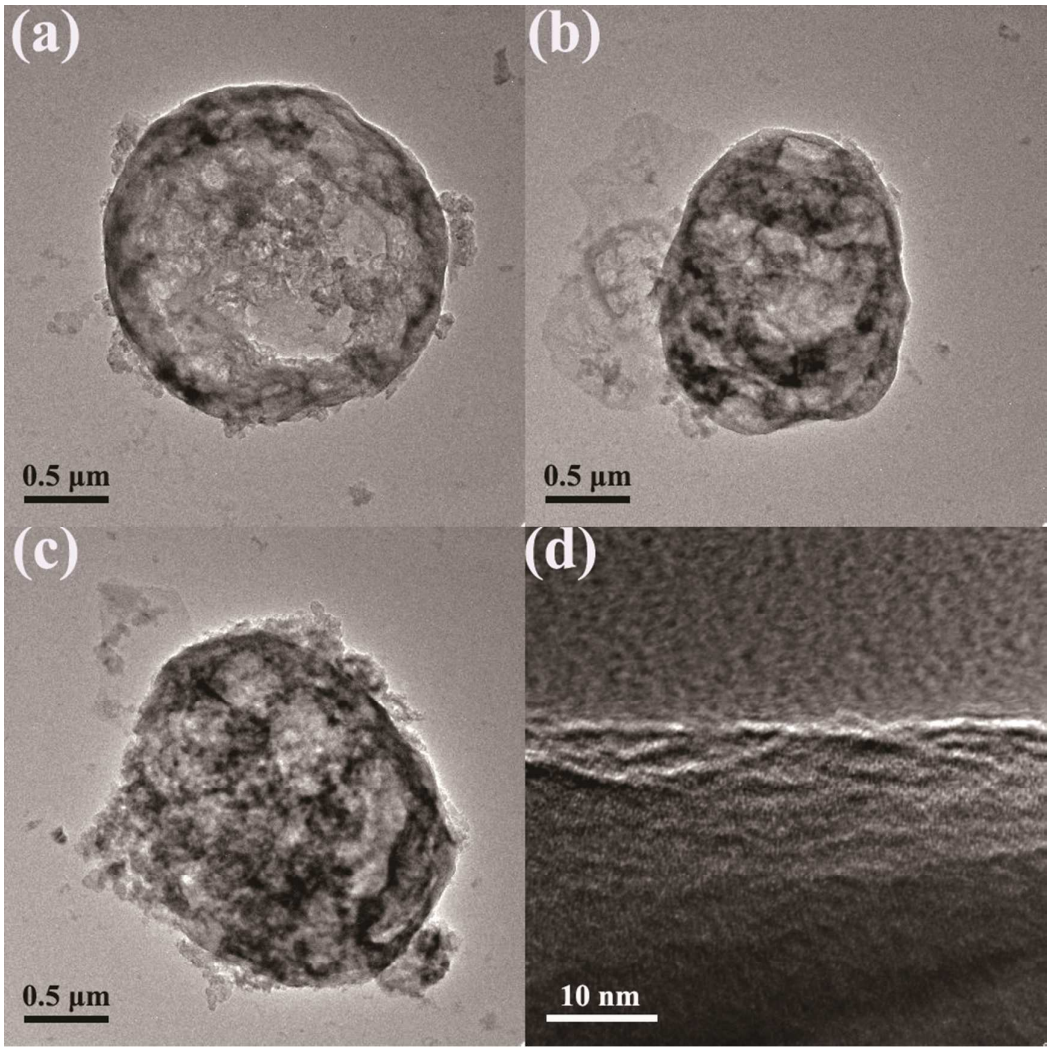

Figure S14. (a), (b) and (c) TEM images of Li_3VO_4@C after 100 cycles. (d)HR-TEM image of Li_3VO_4@C after 100 cycles.

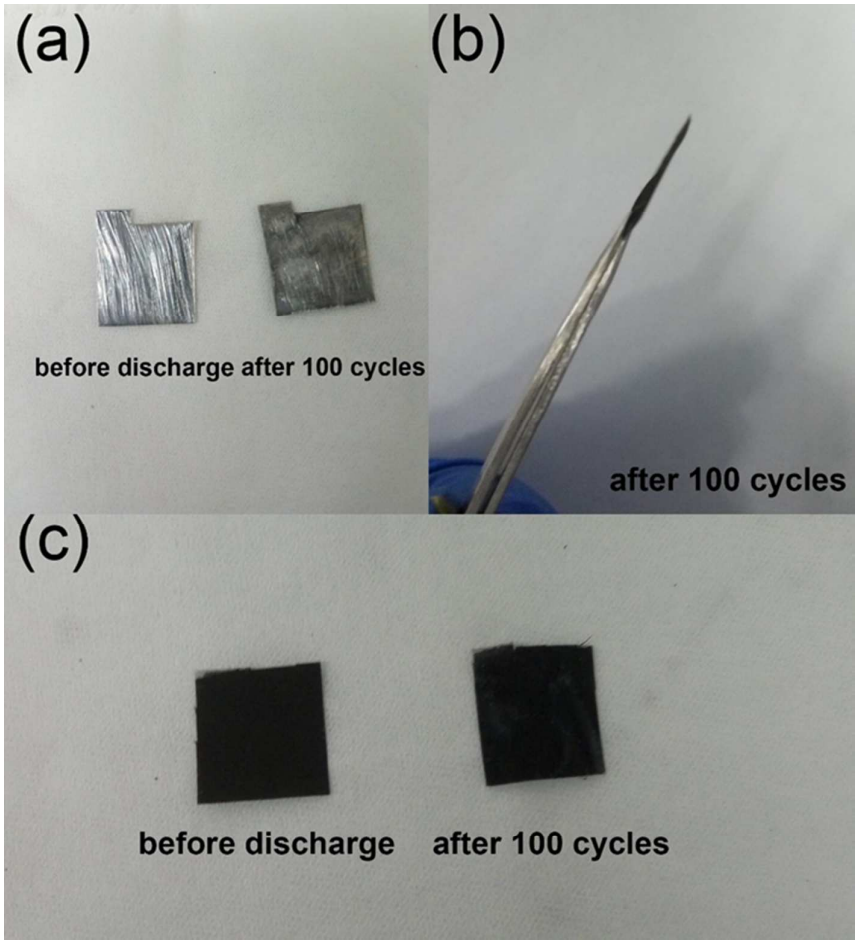

Figure S15. (a) Photographs of Al anodes before discharge (left) and after 100 cycles (right). (b) Side elevation of Li_3VO_4@C electrode after 100 cycles. (c) Photographs of Li_3VO_4@C electrodes before discharge (left) and after 100 cycles (right).

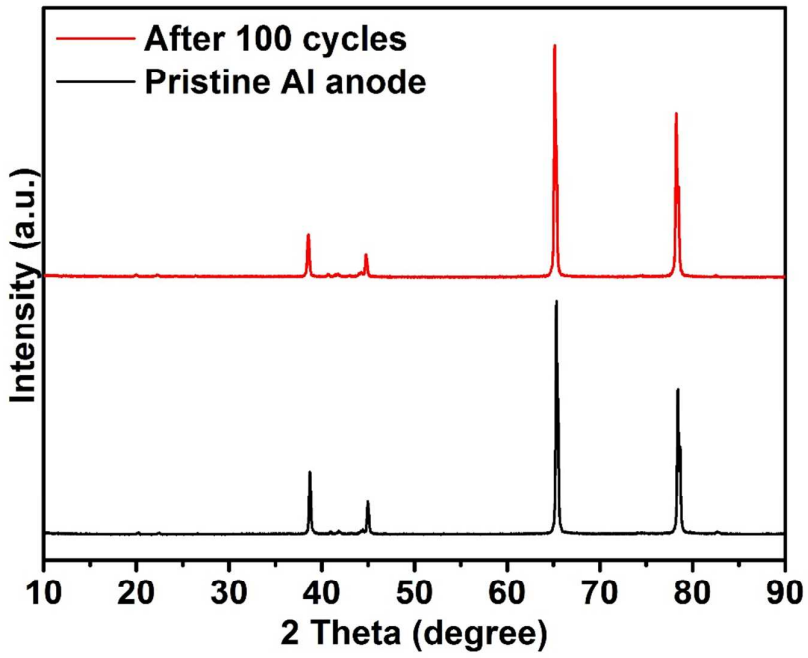

Figure S16. The XRD patterns of Al anode before and after 100 cycles.

Supporting Information References

(1) Sun, X. G.; Fang, Y.; Jiang, X.; Yoshii, K.; Tsuda, T.; Dai, S., Polymer Gel Electrolytes for Application in Aluminum Deposition and Rechargeable Aluminum Ion Batteries. *Chem. Commun.* **2016,** *52,* 292-295.

(2) Lin, M. C.; Gong, M.; Lu, B.; Wu, Y.; Wang, D. Y.; Guan, M.; Angell, M.; Chen, C.; Yang, J.; Hwang, B. J.; Dai, H., An Ultrafast Rechargeable Aluminium-ion Battery. *Nature* **2015,** *520,* 325-328.

(3) Gao, T.; Li, X.; Wang, X.; Hu, J.; Han, F.; Fan, X.; Suo, L.; Pearse, A. J.; Lee, S. B.; Rubloff, G. W.; Gaskell, K. J.; Noked, M.; Wang, C., A Rechargeable Al/S Battery with an Ionic-liquid Electrolyte. *Angew. Chem., Int. Ed.* **2016,** *55,* 9898-8901.

(4) Reed, L. D.; Menke, E., The Roles of V_2O_5 and Stainless Steel in Rechargeable Al–ion Batteries. *J. Electrochem. Soc.* **2013,** *160,* A915-A917.

(5) Jayaprakash, N.; Das, S. K.; Archer, L. A., The Rechargeable Aluminum-ion Battery. *Chem. Commun.* **2011,** *47,* 12610-12612.

(6) Wang, H.; Bai, Y.; Chen, S.; Luo, X.; Wu, C.; Wu, F.; Lu, J.; Amine, K., Binder-free V_2O_5 Cathode for Greener Rechargeable Aluminum Battery. *ACS Appl. Mater. Interfaces* **2015,** *7,* 80-84.

(7) Zhang, K.; Hu, Z.; Liu, X.; Tao, Z.; Chen, J., $FeSe_2$ Microspheres as a High-Performance Anode Material for Na-Ion Batteries. *Adv. Mater.* **2015,** *27,* 3305-3309.

(8) Yang, Y.; Li, J.; He, X.; Wang, J.; Sun, D.; Zhao, J., A Facile Spray Drying Route for Mesoporous Li_3VO_4/C Hollow Spheres as an Anode for Long Life Lithium Ion Batteries. *J. Mater. Chem. A* **2016,** *4,* 7165-7168.

(9) Lee, B.; Lee, H. R.; Yim, T.; Kim, J. H.; Lee, J. G.; Chung, K. Y.; Cho, B. W.; Oh, S. H., Investigation on the Structural Evolutions during the Insertion of Aluminum Ions into Mo_6S_8 Chevrel Phase. *J. Electrochem. Soc.* **2016,** *163,* A1070-A1076.